Journal Name

ARTICLE

Localized effect of PbI$_2$ excess in perovskite solar cells probed by high-resolution chemical-optoelectronic mapping

Jérémy Barbé[a], Michael Newman[a], Samuele Lilliu[b], Vikas Kumar[c], Harrison Ka Hin Lee[a], Cécile Charbonneau[a], Cornelia Rodenburg[c], David Lidzey[b] and W.C. Tsoi[a]

We report the laser irradiation of CH$_3$NH$_3$PbI$_3$ solar cells to generate and control localized PbI$_2$ degradation product. We show that by tuning the laser power and illumination time, we can controllably form a local excess of PbI$_2$. High-resolution advanced multi-mapping techniques are used to highlight the effect of PbI$_2$ on the photophysical and photoelectrical properties in a complete perovskite device. Whereas a thick PbI$_2$ film at the perovskite/hole transport layer interface has a detrimental effect on the photocurrent and photoluminescence, a thin PbI$_2$ film (<20 nm) leads to a significant photocurrent increase, which is ascribed to the passivation of non-radiative defects and reduced charge recombination at the interface. Our findings reveal that laser irradiation is a new approach to understand the effect of PbI$_2$ surface layers and potentially offers a means to passivate trap states and improve PV properties of perovskite devices.

[a.] SPECIFIC - Swansea University, Bay Campus, Fabian Way, Swansea, SA1 8EN, U.K.
[b.] Department of Physics and Astronomy, The University of Sheffield, Hicks Building, Hounsfield Road, Sheffield S3 7RH, U.K.
[c.] Department of Materials Science and Engineering, University of Sheffield, Mappin Street, Sheffield S1 3JD, U.K

INTRODUCTION

Perovskites have generated tremendous interest because of their excellent optoelectronic properties such as high absorption coefficient[1], long carrier lifetime, high carrier mobility[2] and tolerance to defects[3]. Intense research effort has led to a dramatic rise in power conversion efficiency (PCE) of perovskite solar cells (PSCs)[4]. However, despite rapid progress, record PCEs are still far from the Shockley-Queisser limit[5] which suggests that non-radiative recombination plays a key role in the overall efficiency loss. Furthermore, stability issues remain a major challenge for PSCs that needs to be fully addressed before perovskite devices can reach the market[6].

The stoichiometry of perovskites has been shown to have a significant impact on device performance. Several studies have investigated the effect of non-stoichiometric perovskite films containing a deficiency or excess of PbI_2[7,8,9,10,11,12]. The general trend is that a slight excess of PbI_2 is usually beneficial to device performance. This has been observed not only for standard methylammonium lead iodide ($CH_3NH_3PbI_3$) devices[13] but also for mixed perovskites such as $(FAPbI_3)_{0.85}(MAPbBr_3)_{0.15}$[14]. High performance PSCs with more than 21% PCE have been obtained using a triple cation perovskite containing some excess lead iodide[15]. Two main routes have been used to obtain excess PbI_2 phase in the perovskite layer. The first route induces the crystallization of $CH_3NH_3PbI_3$ from a non-stoichiometric $PbI_2:CH_3NH_3I$ ratio. This can be achieved using a one-step synthesis method in which the $PbI_2:CH_3NH_3I$ ratio is tuned directly in the precursor solution[9]. However, changing the composition of the precursor solution from under-stoichiometric (PbI_2 deficient) to over-stoichiometric (PbI_2 excess) can affect the size of the perovskite crystallites formed[10], a feature that complicates the interpretation of the role of embedded PbI_2 phase. A two-step synthesis method has also been used where PbI_2 is first deposited and subsequently exposed to the methylammonium iodide[16,11,17,18]. Here, the overall stoichiometry depends on the length of the second step, as shorter exposure times result in incomplete conversion of PbI_2 to $CH_3NH_3PbI_3$. However, this method usually leads to a less precise control of the film.

The second route uses post-deposition thermal annealing to generate PbI_2 in the already formed $CH_3NH_3PbI_3$ film[19,13]. Thermal annealing induces the decomposition of the perovskite phase to PbI_2, which amount can be controlled by adjusting the annealing time or temperature. Using this method, Du et $al.$ showed that the PbI_2 that forms at grain boundary regions can have a positive effect on device performance, by reducing current-voltage hysteresis and increasing the PCE[19]. However, at higher annealing temperatures, excessive formation of PbI_2 causes resistive losses and poor device performance. Chen et al. reported similar PbI_2 passivation effect after annealing the perovskite film at 150°C for 60 min, but found that longer annealing times deteriorated device performance by introducing excessive PbI_2[13]. One of the drawbacks of such post-deposition thermal annealing processes is the limited control over the amount of PbI_2 that is formed. Furthermore, thermal annealing can also induce secondary effects via modification of the perovskite film crystalline structure.

The reasons for the apparently beneficial effect of a PbI_2 excess are still unclear. Several groups have suggested more favourable energy alignments of the perovskite layer with electron and hole transport layers. Here, it was proposed that PbI_2 can form a type I band alignment with the perovskite, resulting in more efficient charge extraction by energy band matching and decreased interfacial recombination[9,13]. Since PbI_2 was observed to preferentially form at grain boundaries, it was also proposed that a small amount of PbI_2 can passivate grain boundaries, resulting in reduced ion migration[10,8], increased shunt resistance and decreased non-radiative losses[19,14]. However, a consensus on the beneficial role of PbI_2 has not been reached with recent studies suggesting that residual PbI_2 is not required to obtain high performance PSCs, but instead reduces device stability[20,12]. These conflicting results may well arise due to the high sensitivity of PSCs to the precise amount and location of PbI_2 phase in the active layer. In general, the techniques used to control PbI_2 concentration do not provide sufficiently precise control, with small variations in PbI_2 levels having potentially dramatic effects on device operation. Furthermore, such techniques also do not afford any control over the location of excess PbI_2, with PbI_2 believed to form homogeneously throughout the depth of the film. It would clearly be preferential to have control over the location of excess PbI_2, as this could for example allow band alignment/engineering or passivation mechanisms to be exploited at the interfaces of the perovskite layer with the different charge-transporting layers.

To address such issues, we report a laser-induced mechanism that permits precise control over the generation of PbI_2 in a perovskite device stack. We show that when a perovskite device in air is exposed to a laser beam, it is possible to induce a localized structural conversion from $CH_3NH_3PbI_3$ to PbI_2, with this process being finely controlled by adjusting laser power and illumination time. This

technique is used to pattern regions having different PbI_2 content on the same sample with micrometer scale resolution, without modifying crystal structure or grain size. Furthermore, this technique also preferentially generates PbI_2 at the surface of the perovskite (at the interface with the HTL in the inverted device configuration); a feature that may allow a better understanding of the role of PbI_2 at this specific interface to be gained.

A number of groups have used mapping techniques to correlate spatial heterogeneity in lead halide perovskite materials to device performance[14,21]. For example, Eperon et al. found that photocurrent and photoluminescence measurements could be used to understand how the nature of charge-extracting contacts affect recombination losses in a full device structure[22]. However, such techniques do not provide direct information on the chemical or structural properties of the perovskite and need to be interpreted with caution. In our previous work, it was shown that the distribution of PbI_2 degradation products can be measured with micrometer spatial resolution using Raman spectroscopy (RS)[23]. In this paper, we use RS in combination with photocurrent and photoluminescence mapping to unambiguously correlate the local presence of PbI_2 with variations in photophysical and photoelectrical properties in a PSC. Results show that a thin PbI_2 film (< 20 nm) is formed at the perovskite/HTL interface which enhances the photocurrent by passivating defect-states and reducing carrier recombination. The advanced mapping techniques combined with electron microscopy measurements highlight the role played by a localized excess of PbI_2 in a PSC; a result that would be difficult to obtain using other characterization methods.
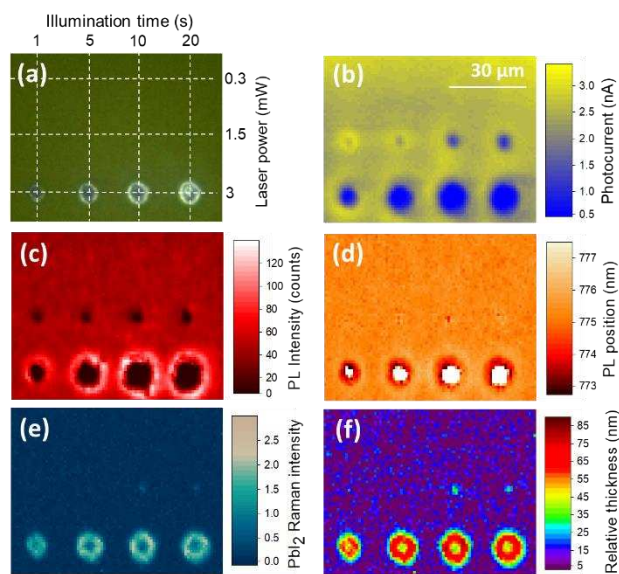
RESULTS

Excess PbI_2 generated by laser irradiation of perovskite solar cells.

All experiments were performed on inverted perovskite solar cells based on the structure glass/ITO/NiO_x/$CH_3NH_3PbI_3$/PCBM/BCP/Ag, where NiO_x is used as a hole transport layer (HTL) and PCBM/BCP as an electron transport layers (ETL). A laser used to generate Raman scattering was also used to deliberately accelerate and control the degradation of the perovskite film within the device stack by varying the laser power and illumination time. The irradiation of samples was performed from the glass side, with the laser light penetrating the device through the transparent ITO and NiO_x layers and being absorbed within the perovskite layer. All irradiation experiments were carried out in air, however photocurrent-PL-Raman maps were

acquired under a N_2 atmosphere to avoid any further degradation by the laser.

Fig. 1a shows an optical microscopy image of several areas that have been irradiated using a laser flux from 0.3 mW to 3 mW, for an illumination time from 1 s to 20 s (equivalent to an energy of 0.3 mJ to 60 mJ). For laser power less than 3 mW, the film appears uniform with no change in film morphology or colour observed. However, when the laser power is increased to 3 mW, a bright halo can be seen around the centre of the irradiated area, which diameter increases with illumination time. This halo cannot be seen for laser power less than 3 mW, even when the illumination time is increased to reach similar or higher dose of incident photons. Indeed, the irradiated spot corresponding to 1.5 mW/20 s received a photon dose that was 10 times higher than the spot corresponding to 3 mW/1 s however the optical microscopy image does not reveal any visual degradation. This indicates that laser power and photon dose have two distinct effects on the transformation of the perovskite layer.

Fig. 1 Laser irradiation of perovskite solar cells using various illumination time and laser power. (a) Optical microscopy image after degradation. **(b)** Photocurrent map. **(c)** Photoluminescence peak intensity map at ~775 nm. **(d)** Photoluminescence peak position. **(e)** PbI_2 Raman integrated intensity (80-140 cm^{-1}). **(f)** PbI_2 film thickness calculated using equation 1. Dimensions of all images are 80 μm x 60 μm.

Photocurrent and photoluminescence maps acquired simultaneously on the same region are shown in Fig. 1b-c. For a laser power of 0.3 mW, no change in photocurrent or PL intensity is apparent, indicating that at this power, the laser did not induce any modification of the structural or optoelectronic properties of the perovskite. Areas irradiated with 1.5 mW laser power are all characterized with a clear drop in PL intensity regardless of the illumination time. However, this

either results in an increase in photocurrent (for 1 s irradiation) or a decrease in photocurrent (10 – 20 s irradiation). For a laser power of 3 mW, we find that all degraded spots are associated with a clear decrease in photocurrent (Fig. 1b), however a halo of slightly higher photocurrent (as compared to the surrounding non-irradiated perovskite) appear at the periphery of irradiated areas. Interestingly, the PL map also indicates a strong decrease in PL emission intensity from the centre of the irradiated spots, which is also surrounded by a halo region from which there is increased emission intensity. This demonstrates that the photo-degradation of the perovskite device by the laser beam is highly dependent on the laser power and illumination time; a process that leads to non-uniform modifications of the optoelectronic properties of the perovskite. Under strong irradiation conditions, a highly degraded region is formed that is characterized by very low PL emission and low photocurrent. This is surrounded by a halo of high photocurrent and high photoluminescence intensity.

Then, Raman mapping were performed on the irradiated regions and plot in Fig. 1e the integrated Raman intensity between 80 cm^{-1} and 140 cm^{-1}, a range which includes the two main peaks of PbI_2 at 96 cm^{-1} and 110 cm^{-1},[23] so that the bright regions of the map reveal areas with high PbI_2 content. It is apparent that the spots treated with 3 mW laser power show PbI_2-rich halo shapes of external diameter comparable to regions characterised with low PL (Fig. 1c) and low photocurrent (Fig. 1b). However when irradiated by the 1.5 mW power laser, the presence of PbI_2 in the perovskite film can only just be detected for illumination times of at least 10 s. Interestingly, changes can be observed by PL and photocurrent mapping from spots that have been exposed using shorter illumination times (< 10 s at 1.5 mW). This indicates that the PL and photocurrent techniques are more sensitive to the photodegradation of the buried perovskite film than is Raman spectroscopy (RS). We note that RS provides direct information regarding the main degradation product of the perovskite (PbI_2), however photoluminescence emission can be challenging to interpret when measuring a device as a number of competing mechanisms may occur simultaneously. For example, free charges in a device at short-circuit will quench the PL[13], however passivation of non-radiative recombination centers can have the opposite effect and induce an increase in PL intensity[24,9]. For this reason, the simultaneous use of photocurrent mapping and Raman mapping is key to understand the physical and chemical changes that happen in a perovskite device as a result of optical irradiation.

To further investigate the correlation between photocurrent, PL and Raman data, Fig. 2a plots a line profile for these different parameters across the area treated with 3 mW/5 s laser irradiation, a region displaying the characteristic halo shape. The PbI_2 Raman profile indicates two maxima distant of 7 μm corresponding to the median diameter of the PbI_2-rich halo. At the center of the spot the intensity of the PbI_2 Raman peak (10^4 counts) is approximately half of that associated to the brightest part of the halo (2 x 10^4 counts); this is higher than outside the halo, where no PbI_2 is measured (0 counts). The outer and inner diameters of the halo are 13 μm and 3 μm, respectively.

Fig. 2 line profiles along a spot area irradiated with high laser power. (a) PbI_2 Raman intensity map for a perovskite device irradiated with 3 mW laser power for 5 s. **(b)** PbI_2 Raman intensity, photocurrent and photoluminescence intensity profiles along the irradiated spot. The dashed lines show the average values of PbI_2 Raman intensity (green line), photocurrent (blue line) and photoluminescence intensity (orange line) outside of the irradiated area.

In recent work, DeQuilettes et al. also observed a similar 10 μm halo of high iodide content after laser irradiation, which was explained by a photo-induced redistribution of iodide ions away from the illuminated area[25]. This effect was observed after a rather long illumination time of a few hundreds of seconds. However, in Fig. 1e the PbI_2 halo can be observed after 1 s illumination time at 3 mW laser power, a finding that makes a hypothesis of iodide redistribution less likely. Furthermore, because of the high laser intensity used, we cannot exclude the PbI_2 formation resulting from a heating effect caused by laser irradiation. Indeed, if we consider the laser beam intensity to have a Gaussian shape, the PbI_2 halo may be formed by

the beam tails provided they have sufficient intensity to degrade the perovskite to PbI_2. At the center of the spot, the PbI_2 could further decompose into a third phase, possibly polyiodide compounds[26], which would explain the non-gaussian shape of the PbI_2 Raman profile.

The formation of PbI_2 after laser irradiation can be correlated with variations in photocurrent and PL intensity. In Fig. 2b, we observe that the PL intensity and photocurrent drop in all areas of high PbI_2 intensity (region 1), which is ascribed to reduced perovskite content and high series resistance of PbI_2 in this region. Interestingly, the lowest value of photocurrent isn't null, inferring that the cell stack remains functional over the entire laser-treated spot area. In region of moderate PbI_2 content (region 2), the PL raises significantly to reach up to twice the average value of the PL in non-degraded regions, whereas the photocurrent is still reduced as compared to the average value, thus showing a high PL-low photocurrent anticorrelation. Then, in region of low PbI_2 content, immediately adjacent to the PbI_2 halo (region 3), both the PL and photocurrent are increased as compared to their average values, thus showing a high PL-high photocurrent correlation. From the map shown in Fig. 1b, the photocurrent was measured to increase of up to 16% around spots degraded with 3 mW laser power. The combination of all three sets of data emphasizes the complex relation between the local formation of PbI_2 and device performance; it also suggests the occurrence of other transformations than the conversion of $CH_3NH_3PbI_3$ to PbI_2 inside the perovskite layer by result of the laser radiation which may be associated to the PL and photocurrent profiles collected, as discussed further on.

Quantification of excess PbI_2 by Raman spectroscopy

Raman spectroscopy is a powerful qualitative technique but also a quantitative technique that allows thin film thickness to be determined with high accuracy. Recently, Raman spectroscopy has been utilized to determine the thickness of organic thin films down to 3 nm with an error margin of 20%[27]. To quantify the amount of crystalline PbI_2 present in the complete perovskite device stack, we calibrated our Raman system by preparing PbI_2 thin films having various thicknesse. Raman spectra of PbI_2 films measured with 0.15 mW laser power and 10 s acquisition time are shown in Fig. S2b. After baseline subtraction, we observe a systematic decrease in intensity of PbI_2 peaks as the PbI_2 concentration/thickness is decreased; a property that allows us to determine the limit of detectability of PbI_2 by Raman. The minimum detectable thickness by Raman is 18 ± 5 nm (corresponding to 0.1 M PbI_2 concentration). We then plot the PbI_2
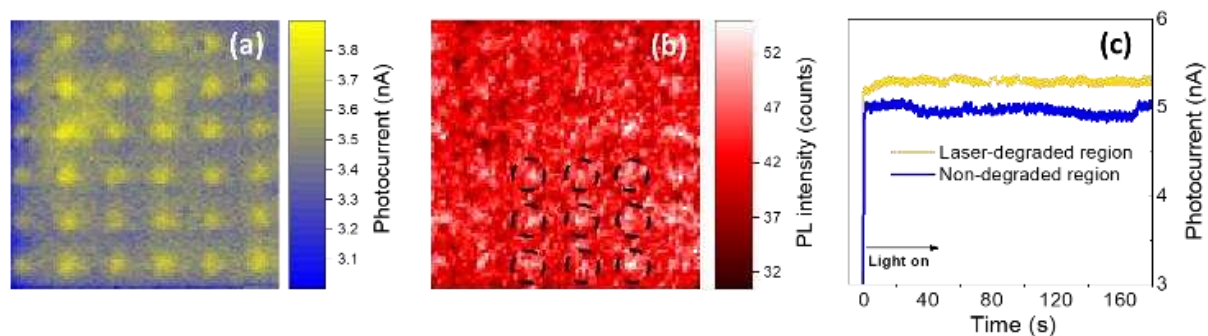
Raman intensity (integrated intensity between 80 cm^{-1} and 140 cm^{-1}) as a function of film thickness (Fig. S2c). This indicates a non-linear dependence of the Raman intensity versus thickness which can be used to estimate the PbI_2 effective thickness within the layer stack and obtain a PbI_2 relative thickness map after laser irradiation, as shown in Fig. 1f.

From this map, we measured a minimum PbI_2 thickness of 25 ± 5 nm after laser irradiation having a power of 1.5 mW and 10 s illumination time (values below 25 ± 5 nm correspond to background noise). We note that a 25 nm-thick PbI_2 film would act as an insulating layer at the interface with the HTL and would thus block charge transfer[10]. This suggests that as soon as PbI_2 is detected by Raman in the device configuration, it is already too thick to be beneficial for device performance, a result confirmed by the photocurrent map that shows a decrease in photocurrent in all areas in which PbI_2 was detected by Raman spectroscopy. In contrast, in areas of high photocurrent (e.g. for an irradiated spot created using a 1.5 mW laser for 1 s), the PbI_2 Raman signal cannot be detected at these measurement settings, indicating that the PbI_2 effective thickness is less than 18 ± 5 nm. The sensitivity of Raman to PbI_2 could most likely be enhanced by using higher laser power or longer acquisition times, however this measurement condition would likely damage the perovskite film and induce further formation of PbI_2, as shown in our previous work[23]. The maximum PbI_2 effective thickness measured within the bright PbI_2 halo is estimated to be around 80 nm. This demonstrates that Raman spectroscopy is a non-destructive technique that can be used to quantitatively determine the quantity and distribution of PbI_2 formed during photodegradation of perovskite devices, with this technique having micrometer lateral resolution and relatively high sensitivity down to an effective PbI_2 thickness of approximately 20 nm. Raman spectra of fresh PSCs with various excess of PbI_2 incorporated directly in the precursors solution were also measured (Fig. S4). The spectra show typical weak and broad bands of $CH_3NH_3PbI_3$ at 250 cm^{-1} and 110 cm^{-1}, however no PbI_2 signal is detected; a result that confirms that PbI_2 phase is present at concentrations that cannot be detected by Raman using our experimental settings.

Improved optoelectronic properties of perovskite solar cells after laser irradiation with reduced power

We have previously observed that laser irradiation at relatively high power density can accelerate the photodegradation of perovskite devices and generate PbI_2 at a perovskite/NiO_x interface. We now investigate the effect of reduced laser irradiation on the local

Fig. 3 Photo-electrical measurements of perovskite solar cell irradiated with laser power 0.3 mW for 120 s. **(a)** Photocurrent map on a 120 µm x 120 µm region. **(b)** Photoluminescence intensity at ~775 nm. **(c)** Stabilized photocurrent at short-circuit measured on irradiated (yellow) and non-irradiated (purple) regions.

photocurrent and photoluminescence behaviours in a PSC. To do this, an array of 6x6 spots separated by 20 µm was irradiated using a laser

power of 0.3 mW for 120 s. As perovskites are known to be largely inhomogeneous at the micrometer scale[28], the same irradiation conditions were applied to confirm that the observed laser-induced effects are not due to specific localized microstructure or defects. In Fig. 3a, a clear increase in photocurrent can be observed at regions in which the perovskite device was irradiated, with an average enhancement in photocurrent of 7% compared to non-irradiated regions. The stabilized photocurrent at short-circuit shown in Fig. 3c indicates the same enhancement in photocurrent from irradiated regions, even after 180 s of illumination. This indicates that optoelectronic/chemical changes in the perovskite device after irradiation are permanent and don't result from transient mechanisms such as ion migration. The PL intensity map at 775 nm (Fig. 3b) indicates a slight increase in PL intensity from the irradiated regions. Besides, in contrast to results shown in Fig. 1 (higher laser powers), no halo surrounding irradiated regions is detected. Raman mapping did not detect a PbI₂ signal, from either the irradiated or non-irradiated regions, a result that suggests that significant quantities of PbI₂ (> 20 nm effective thickness) were not created under these specific irradiation conditions.

Impact of laser irradiation on the microstructure of the perovskite layer
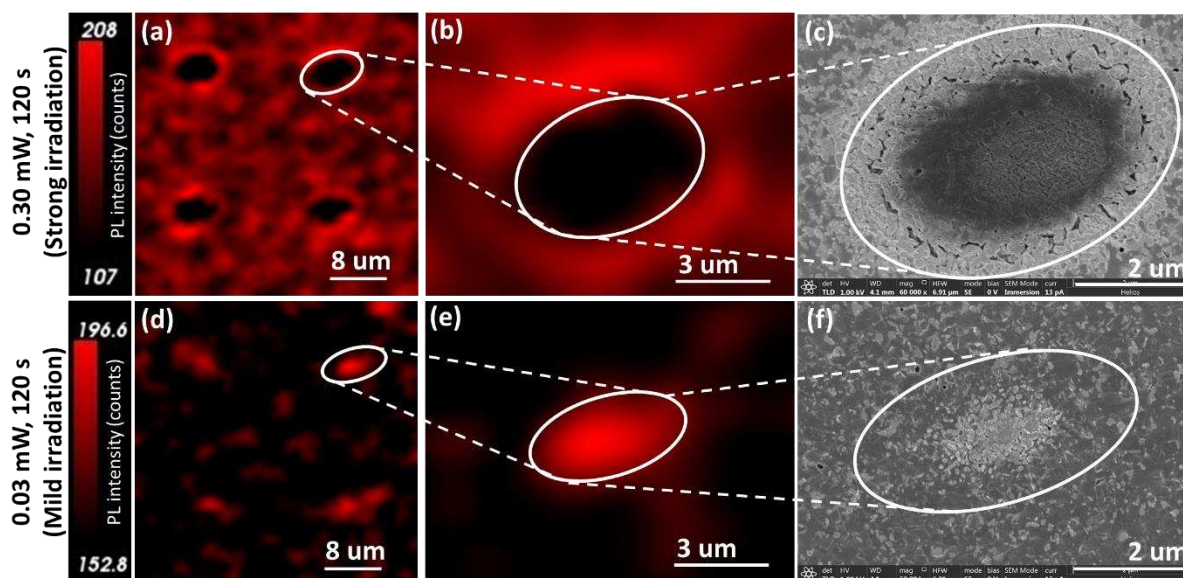
As small quantities of PbI₂ in a device structure are challenging to probe by RS, scanning electron microscopy (SEM) and energy dispersive spectroscopy (EDS) were used to gain further insights into the perovskite microstructure and distribution of PbI₂. Here, CH₃NH₃PbI₃ thin films were fabricated onto a glass/ITO/NiOₓ substrate and exposed to laser irradiation in air. As the perovskite films were directly exposed to air during the irradiation and were not covered by

PCBM/BCP/Ag top layers, reduced laser powers of 0.3 mW and 0.03 mW were used to obtain similar degradation levels as used in devices degraded with 3 mW (strong irradiation) and 0.3 mW (mild irradiation), respectively.

Under strong irradiation conditions, the PL intensity map shown in Fig. 4a confirms the presence of highly degraded regions characterized by quenched PL that are surrounded by a halo of increased PL intensity. It can be seen from the top-view SEM image shown in Fig. 4c that there is non-uniform degradation on the film surface, with a dark region of highly degraded perovskite film located at the centre of the spot that is surrounded by a bright halo of high PbI₂ content. This finding is also confirmed by EDS measurements (Fig. S5b). The diameter of the PbI₂ halo as determined by SEM is around 6-7 µm; a finding in good agreement with the Raman profile shown in Fig. 2b.

We compare the photoluminescence intensity map and the top-view SEM picture in Fig. 4c. Interestingly, the region in which PL is quenched corresponds almost perfectly to the PbI₂ halo and dark central region. The region of increased PL intensity is rather located just at the outer edge of the PbI₂ halo, as was observed in device structure shown in Fig. 1. From the high-magnification SEM image (Fig. S5a), this region corresponds to a change in perovskite morphology (as compared to unaffected region), where small bright grains considered to be PbI₂ are formed at perovskite grain boundaries, as observed by other groups[13,14]. This confirms our assumption that a small quantity of PbI₂ is formed just outside the halo, although it is not detectable by RS (which corresponds to region 3 in Fig. 2b).

Under mild irradiation conditions, we find that the PL emission from the directly irradiated regions undergoes a uniform increase in intensity (see Fig. 4d and 4e). From the SEM image shown in Fig. 4f, it can be seen bright features at the centre of the illumination spot, which EDS measurements (Fig. S5d) indicate correspond to PbI₂.

Fig. 4 Perovskite film microstructure after laser irradiation. (a) and **(b)** Photoluminescence intensity maps at 775 nm and **(c)** top-view SEM images of perovskite films on NiO$_x$/ITO/glass substrates after laser degradation with 0.30 mW laser power for 120 s (equivalent of 3 mW for devices). **(d)** and **(e)** Photoluminescence intensity maps at 775 nm and **(f)** top-view SEM images of perovskite films on NiO$_x$/ITO/glass substrates after laser degradation with 0.03 mW laser power for 120 s.

However, we also find that there is a significant carbon content (17.4 wt%) at the irradiated region, which is just slightly lower than that found at non-irradiated regions (21 wt% in Fig. S5b and d). This indicates that non-degraded perovskite material is still present underneath the overlying PbI$_2$ layer (at 10 kV, the e$^-$ penetration depth of the primary electron beam is around 600 nm with 90% of the beam energy dissipated in the top 200 nm thickness). This indicates that under mild laser irradiation conditions, a thin PbI$_2$ film forms at the surface of the perovskite layer as a result of photodegradation. EDS measurements indicate that this PbI$_2$ film is very thin as unaffected perovskite is still measured underneath, on the contrary to regions having thick PbI$_2$ film (Fig. S5b). This is also in good correlation with our quantification of the PbI$_2$ amount by RS showing that the PbI$_2$ effective thickness is less than 20 nm when PbI$_2$ peaks are not distinguishable from background noise in the Raman spectra. Such thin PbI$_2$ film acts as a passivation layer for non-radiative defects on top of the perovskite surface, as revealed by the PL enhancement observed at irradiated spots in Fig. 4d. In the device structure, we also believe that a thin PbI$_2$ passivation layer can be formed at the interface between the perovskite and NiO$_x$ HTL, which is sufficiently thin that it cannot be detected by RS.
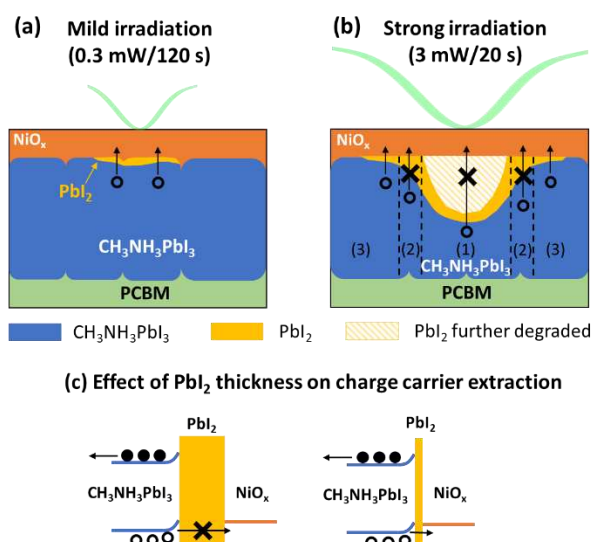
DISCUSSION

From these results, it is apparent that the formation of PbI$_2$ that occurs as a product of perovskite photodegradation has a significant effect on PSCs performance, and the concentration of PbI$_2$ generated within the device stack determines its effect on the local photocurrent. In scheme 1, we propose a mechanism of PbI$_2$ passivation at the perovskite/NiO$_x$ interface consistent with our observations in this work. For strong laser illumination (3 mW), both hypothesis of iodide redistribution or thermal degradation result in the formation of a thick PbI$_2$ halo, having a detrimental effect on the local photocurrent. Here, a small amount of PbI$_2$ is most likely located just outside the degradation halo, although this cannot be detected by Raman. Indeed, in Fig. S5a PbI$_2$ clusters (identifiable as bright features) can be observed that correlate with areas of high PL intensity and enhanced photocurrent. Under mild irradiation conditions, a very thin layer of PbI$_2$ appears to form at the centre of the laser spot and also causes similar effects (increased local PL intensity and photocurrent). Our calibration using Raman spectroscopy indicates the effective thickness of the PbI$_2$ film to be less than 20 nm. It appears therefore that excess PbI$_2$ results in enhanced photocurrent when its effective thickness is less than 20 nm, whether it is created using strong or mild laser irradiation conditions.

The correlation between higher photoluminescence and higher photocurrent in regions where a thin PbI$_2$ layer is formed supports the hypothesis that PbI$_2$ acts as a passivation layer at the perovskite/NiO$_x$ interface[10]. As discussed earlier, PbI$_2$ is able to create a better electronic coupling between the active layer and the extraction layer, leading to reduced PL emission intensity as carriers will be extracted

Scheme 1 mechanisms of PbI₂ passivation at perovskite/NiOₓ interface after laser irradiation. (a) for mild laser irradiation and **(b)** for strong laser irradiation. **(c)** Effect of PbI₂ thickness on charge carrier extraction and passivation at perovskite/NiOₓ interface.

from the device before they recombine in the perovskite. We note that Eperon et al. observed a slight anti-correlation between local PL intensity and photocurrent that was ascribed to variations in electronic coupling between the perovskite layer and the top contact[22]. However, PbI₂ can also act as a passivation interfacial layer for non-radiative defects that will instead increase overall PL yield; a situation that appears in good agreement with our findings (indicated in region 3 of Fig. 2b and Scheme (1)).

It is clear however that other mechanisms may also be important; for example, photocurrent enhancement may result from photothermally-induced recrystallization of the perovskite. Indeed, recent findings have revealed that exposure to nanosecond pulsed UV laser irradiation can induce rapid crystal phase reconstruction of a perovskite, and result in increased PL intensity and lifetime[29]. We note that in these measurements the perovskite underwent a tetragonal to cubic phase transition, which was revealed by the appearance of Raman peaks at 85 cm⁻¹, 139 cm⁻¹ and 280 cm⁻¹ (with the highest energy mode assigned to methylammonium). However, none of such peaks were observed here, indicating that the perovskite crystal structure most likely remains unchanged in our experiments.
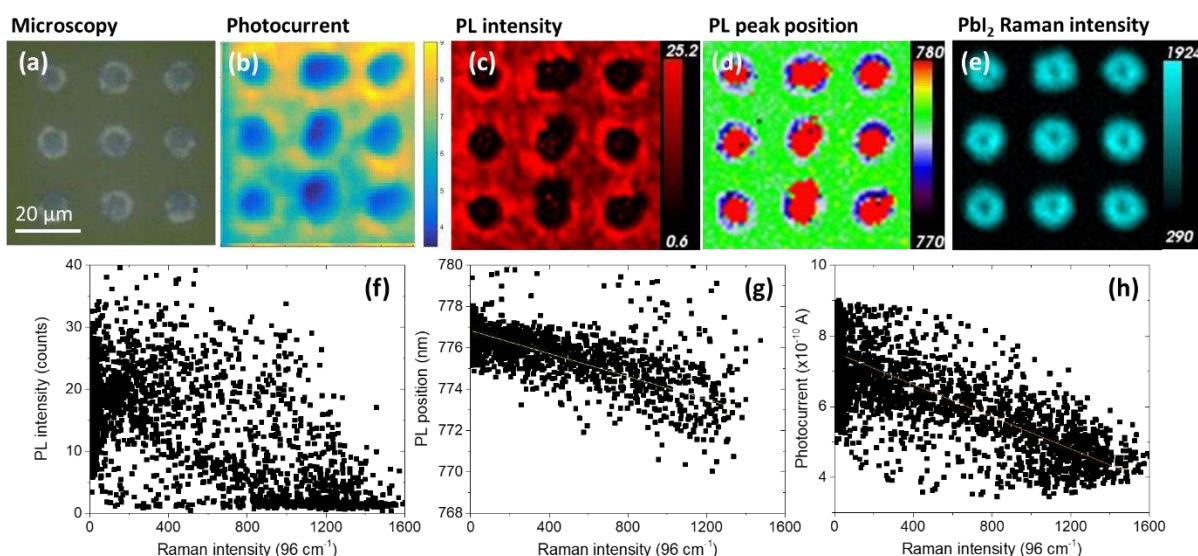
Although the mechanisms by which PbI₂ passivates perovskite defects is still a matter of debate, it is generally accepted that passivation of surface and grain boundaries in perovskite can decrease non-radiative defects and trap states, and result in increased PL intensity and lifetime[14]. Chen et al. suggested that the presence of PbI₂ at the interface between the perovskite and a hole transport material can

affect the alignment of band edges and induce an upward bending of the perovskite conduction band. This band bending would reduce interfacial recombination by pushing electrons away from the interface[13]. Recently, Gujar et al. reported that a small fraction of PbI₂ embedded in a perovskite film reduces non-radiative recombination and increases PL intensity, but found that a higher fraction of PbI₂ had a detrimental effect on PL intensity[20]. This finding is in good agreement with our results that demonstrate that PL enhancement is correlated with the presence of small concentration of PbI₂, however highly degraded perovskite with higher PbI₂ effective thickness are correlated with reduced PL intensity.

Finally, the advanced multi-mapping techniques used in this work allow us to extract additional information resulting from the large data-sets that are collected. For example, Fig. 5f-g plot the PL peak intensity and position as a function of PbI₂ Raman intensity, following irradiation of 9 different regions with 50% laser power for 10 s. Here each pixel in the photoluminescence maps (Fig. 5c-d) is correlated with the corresponding pixels of the PbI₂ Raman intensity map (Fig. 5e). It can be seen that the PL intensity vs. PbI₂ content are not clearly correlated. Indeed, Eperon et al. also obtained a poor correlation between the PL intensity and photocurrent[22]. This indicates that PL intensity in a perovskite film or device is likely to depend on many factors that relate to bulk and interface properties, and likely to the surface roughness of the film. It can be seen however that the PL peak position undergoes a linear blue-shift as the PbI₂ content is increased, confirming that such techniques are quantitative and sensitivetools to investigate perovskite degradation and PbI₂ formation. The reasons for the PL blue-shift with increasing PbI₂ content are still unclear but are also likely to result from the passivation of defects near the band tail states in perovskite[30]. Finally, Fig. 5h shows that a large excess of PbI₂ (detectable by RS) is usually responsible for lower photocurrent owing to the creation of resistive pathways within the perovskite layer.

CONCLUSIONS

We have shown that high-resolution multimapping techniques can be used to correlate the effect of localized PbI₂ degradation product to local photocurrent. The amount of PbI₂ formed by laser-degradation in the active layer can be both tuned by varying incident laser power and illumination time, but also detected using Raman spectroscopy providing that enough PbI₂ is formed.

Fig. 5 Multi-mapping of perovskite device degraded in air with laser power 15 mW for 10 s. **(a)** Microscopy image, **(b)** photocurrent, **(c)** PL intensity, **(d)** PL peak position, **(e)** PbI_2 Raman integrated intensity. Data points from maps were extracted to plot **(f)** PL intensity **(g)** PL position and **(h)** photocurrent vs. PbI_2 Raman intensity (at 96 cm^{-1}).

For specific "mild" irradiation conditions, an increase of the photocurrent is observed at irradiated areas; a finding that correlates with an increase in photoluminescence intensity. We ascribe this effect to passivation from a thin PbI_2 surface layer (< 20 nm) that reduces non-radiative pathways at the perovskite/NiO_x interface. These findings give a better understanding of the localized effect of PbI_2 excess formed within methylammonium lead iodide complete device stack. In future work, it will be necessary to study the effect of laser irradiation on the entire cell area to investigate the potential of this technique for improving the macroscopic performance of perovskite solar cells. Besides, potential instability issues due to excess PbI_2 phase in the perovskite film could be monitored by using the advanced multi-mapping technique described[20,12,31].

METHODS

Materials All materials were used without purification. Anhydrous dimethyl sulfoxide (DMSO), *N,N*-dimethylformamide (DMF), anhydrous ethanol, anhydrous chlorobenzene, anhydrous ethanolamine, anhydrous 2-methoxyethanol, nickel acetate (Ni-acc, 98%) were purchased from Sigma-Aldrich. Methylammonium iodide (MAI) was purchased from Dyesol and lead iodide (PbI_2, 99.99%) was purchased from TCI. The electron transport material [6,6]-phenyl-C$_{61}$ butyric acid methyl ester (PCBM) was obtained from Solenne BV while bathocuproine (BCP, 99.8%) was purchased from Ossila. To prepare the NiO_x solution, 0.2 M solution of nickel acetate tetrahydrate was dissolved in a 1:0.012 volume ratio of 2-methoxyethanol:ethanolamine and stirred for 1 h at 60°C. $CH_3NH_3PbI_3$ precursor solution was prepared by mixing CH_3NH_3I and PbI_2 (1:1.05 molar ratio) in DMF/DMSO (4:1 volume ratio) with a concentration of 804 mg mL^{-1} at 60°C for 2 h. PCBM was dissolved in chlorobenzene with concentration 20 mg.ml^{-1} and stirred overnight at 60°C. BCP was dissolved in anhydrous ethanol with concentration 0.5 mg.ml^{-1}. All solutions were filtered with 0.45 μm PTFE syringe filters.

Perovskite solar cell fabrication and testing 15 Ω.□$^{-1}$ ITO/glass substrates (Lumtec) were sequentially cleaned with detergent in DI water, acetone, and isopropyl alcohol in an ultrasonic bath. They were then dried with N_2 and exposed to O_2 plasma for 10 min. ~20 nm-thick NiO_x layer was deposited via spin-coating at 4000 rpm for 30 s followed by 30 min sintering at 250°C. Subsequent layers were prepared under nitrogen in a glove box. The perovskite precursor solution was spin cast at 4000 rpm for 30 s. Chlorobenzene was drop-cast onto the rotating sample after 15 s to promote crystallization. After 10 min drying, the perovskite films were annealed at 100°C for 10 min. After cooling, the PCBM solution was spin-coated onto the $CH_3NH_3PbI_3$ layer at 4000 rpm for 30 s, followed by spin-coating the BCP solution at 6000 rpm for 20 s. The thickness of the perovskite and PCBM layers were measured to be 380 nm and 60 nm, respectively. The thickness of the BCP film was too thin to be measured by profilometry or SEM. Finally, a 100 nm thick silver counter electrode

was evaporated at 10^{-4} Torr using an Edwards 306 thermal evaporator, forming devices with an active area of 0.15 cm^2.

Crystalline PbI_2 films were prepared on glass substrates by spin-coating solutions of PbI_2 in DMF with concentrations from 0.01 M to 1 M to adjust the film thickness, followed by annealing at 70°C for 10 min. Films thickness was measured by profilometry and tapping mode atomic force microscopy (AFM).

Current density–voltage (J–V) characterization was performed using a Keithley 2400 source-meter unit under 0.8 sun illumination using a Newport 92193A-1000 solar simulator. Current-voltage sweeps were performed from both V_{OC}-to-J_{SC} and vice versa at a rate of 0.1 V s^{-1}.

Photocurrent-photoluminescence-Raman mapping Multi-mapping experiments were performed using a Renishaw Invia Raman system in backscattering configuration, as shown in Fig. S1. The sample was mounted in an electrical/environmental chamber (LTS420E, Linkam Scientific Instrument) attached to a motorized stage (100 nm step resolution). A laser excitation at 532 nm and a 50x long objective were used (NA = 0.50, spot size ~1 μm). Photocurrent and photoluminescence maps were acquired simultaneously at laser power of 30 nW (3000 mW.cm^{-2}, 30 suns) and acquisition time of 0.2 s for each measurement spot to perform measurements without affecting the perovskite layer. This was found to be the minimum intensity required to measure the photocurrent with a good signal-to-noise ratio.

The stage was translated in x and y directions to map the photocurrent (short-circuit current) and PL spectra from each spot. To acquire the photocurrent (also called LBIC for laser beam-induced current[32]), the device electrodes were connected to a lock-in amplifier (Stanford Research SR830) with the laser beam chopped at a frequency of 134 kHz. A source-meter unit (Keithley 236) was used to measure the stabilized short-circuit current at specific regions of the perovskite cells. Raman measurements were also performed using a laser power of 0.15 mW and acquisition time of 10 s. All laser degradations/irradiations were performed in air, whereas photocurrent-PL-Raman mapping were performed under N_2.

Electron microscopy

To avoid any damage due to electron beam, a FEI Helios NanoLab G3 UC low voltage SEM was used to image $CH_3NH_3PbI_3$ perovskite thin films. All samples were imaged using a through-lens (TLD)

detector at a working distance of ~4.1 mm with a beam current of 13 pA and an accelerating voltage of 1 kV. Compositional analysis was performed using energy dispersive X-ray spectroscopy (EDX) using the FEI Helios NanoLab equipped with an Oxford EDX detector and the data were collected with an accelerating voltage of 10 keV and a beam current of 25 pA.

ASSOCIATED CONTENT

Experimental set-up used for Raman-photocurrent-photoluminescence mapping, Raman spectra of PbI_2 thin films on glass with different thicknesses, Raman spectra of $MAPbI_3$ films on ITO/glass substrates prepared with different amounts of PbI_2 excess, high and low magnification SEM top-view images of irradiated perovskite films.
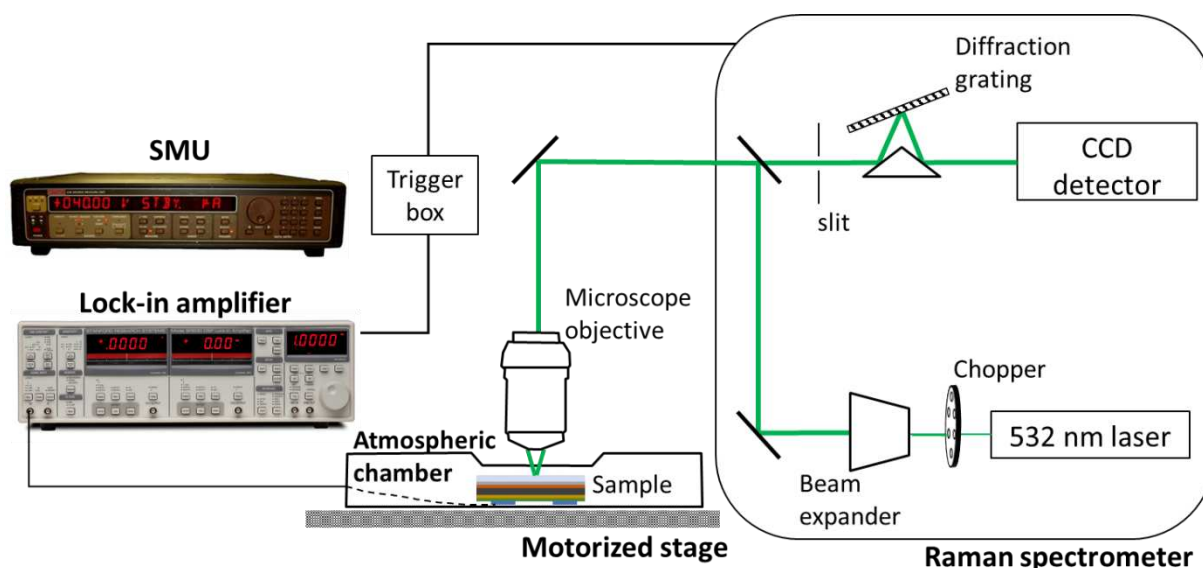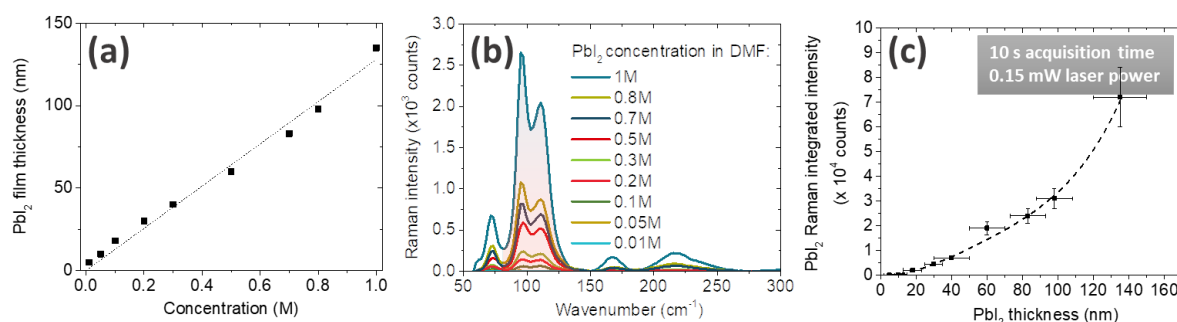
ACKNOWLEDGMENTS

REFERENCES

1   S. De Wolf, J. Holovsky, S. J. Moon, P. Loper, B. Niesen, M. Ledinsky, F. J. Haug, J. H. Yum and C. Ballif, *J. Phys. Chem. Lett.*, 2014, **5**, 1035–1039.

2   S. D. Stranks, S. D. Stranks, G. E. Eperon, G. Grancini, C. Menelaou, M. J. P. Alcocer, T. Leijtens, L. M. Herz, A. Petrozza and H. J. Snaith, *Science*, 2014, **341**, 341–345.

3   K. X. Steirer, P. Schulz, G. Teeter, V. Stevanovic, M. Yang, K. Zhu and J. J. Berry, *ACS Energy Lett.*, 2016, **1**, 360–366.

4   J.-P. Correa-Baena, A. Abate, M. Saliba, W. Tress, T. Jesper Jacobsson, M. Grätzel and A. Hagfeldt, *Energy Environ. Sci.*, 2017, **10**, 710–727.

5   W. E. I. Sha, X. Ren, L. Chen and W. C. H. Choy, *Appl. Phys. Lett.*, 2015, **106**, 221104.

6   T. A. Berhe, W.-N. Su, C.-H. Chen, C.-J. Pan, J.-H. Cheng, H.-M. Chen, M.-C. Tsai, L.-Y. Chen, A. A. Dubale and B.-J. Hwang, *Energy Environ. Sci.*, 2016, **9**, Advance Article.

7   S. Wang, W. Dong, X. Fang, Q. Zhang, S. Zhou, Z. Deng, R. Tao, J. Shao, R. Xia, C. Song, L. Hu and J. Zhu, *Nanoscale*, 2016, **8**, 6600–6608.

8   Y. C. Kim, N. J. Jeon, J. H. Noh, W. S. Yang, J. Seo, J. S. Yun, A. Ho-baillie, S. Huang, M. A. Green and J. Seidel, *Adv. Energy Mater.*, 2016, **6**, 1502104.

9   C. Roldán-Carmona, P. Gratia, I. Zimmermann, G. Grancini, P. Gao, M. Graetzel and M. K. Nazeeruddin, *Energy Environ.*

Sci., 2015, **8**, 3550–3556.

10   T. J. Jacobsson, J. P. Correa-Baena, E. Halvani Anaraki, B. Philippe, S. D. Stranks, M. E. F. Bouduban, W. Tress, K. Schenk, J. Teuscher, J. E. Moser, H. Rensmo and A. Hagfeldt, *J. Am. Chem. Soc.*, 2016, **138**, 10331–10343.

11   D. H. Cao, C. C. Stoumpos, C. D. Malliakas, M. J. Katz, O. K. Farha, J. T. Hupp and M. G. Kanatzidis, *APL Mater.*, 2014, **2**, 1–8.

12   F. Liu, Q. Dong, M. K. Wong, A. B. Djurišić, A. Ng, Z. Ren, Q. Shen, C. Surya, W. K. Chan, J. Wang, A. M. C. Ng, C. Liao, H. Li, K. Shih, C. Wei, H. Su and J. Dai, *Adv. Energy Mater.*, 2016, **6**, 1–9.

13   Q. Chen, H. Zhou, T. Bin Song, S. Luo, Z. Hong, H. S. Duan, L. Dou, Y. Liu and Y. Yang, *Nano Lett.*, 2014, **14**, 4158–4163.

14   S. Chen, X. Wen, J. S. Yun, S. Huang, M. Green, N. J. Jeon, W. S. Yang, J. H. Noh, J. Seo, S. Il Seok and A. Ho-Baillie, *ACS Appl. Mater. Interfaces*, 2017, **9**, 6072–6078.

15   M. Saliba, T. Matsui, J.-Y. Seo, K. Domanski, J.-P. Correa-Baena, M. K. Nazeeruddin, S. M. Zakeeruddin, W. Tress, A. Abate, A. Hagfeldt and M. Grätzel, *Energy Environ. Sci.*, 2016, **9**, 1989–1997.

16   Q. Chen, H. Zhou, Z. Hong, S. Luo, H. Duan, H. Wang, Y. Liu, G. Li and Y. Yang, *J. Am. Chem. Soc.*, 2014, **136**, 622–625.

17   Z. Xiao, C. Bi, Y. Shao, Q. Dong, Q. Wang, Y. Yuan, C. Wang, Y. Gao and J. Huang, *Energy Environ. Sci.*, 2014, **7**, 2619–2623.

18   D. Zhao, M. Sexton, H. Y. Park, G. Baure, J. C. Nino and F. So, *Adv. Energy Mater.*, 2015, **5**, 1–5.

19   T. Du, C. Burgess, J. Kim, J. Durrant, J. Zhang and M. McLachlan, *Sustain. Energy Fuels*, 2017, 119–126.

20   T. P. Gujar, T. Unger, A. Schönleber, M. Fried, F. Panzer, S. van Smaalen, A. Köhler and M. Thelakkat, *Phys. Chem. Chem. Phys.*, 2017, **85**, 605–614.

21   S. Y. Leblebici, L. Leppert, Y. Li, S. E. Reyes-Lillo, S. Wickenburg, E. Wong, J. Lee, M. Melli, D. Ziegler, D. K. Angell, D. F. Ogletree, P. D. Ashby, F. M. Toma, J. B. Neaton, I. D. Sharp and A. Weber-Bargioni, *Nat. Energy*, 2016, **1**, 1–7.

22   G. E. Eperon, D. Moerman and D. S. Ginger, *ACS Nano*, 2016, **10**, 10258–10266.

23   K. E. A. Hooper, H. K. H. Lee, M. J. Newman, S. Meroni, J. Baker, T. M. Watson and W. C. Tsoi, *Phys. Chem. Chem. Phys.*, 2017, **19**, 5246–5253.

24   F. Jiang, Y. Rong, H. Liu, T. Liu, L. Mao and W. Meng, *Adv. Funct. Mater.*, 2016, **26**, 8119–8127.

25   D. W. DeQuilettes, W. Zhang, V. M. Burlakov, D. J. Graham, T. Leijtens, A. Osherov, V. Bulović, H. J. Snaith, D. S. Ginger and S. D. Stranks, *Nat. Commun.*, , DOI:10.1038/ncomms11683.

26   P. Pistor, A. Ruiz, A. Cabot and V. Izquierdo-Roca, *Sci. Rep.*, 2016, **6**, 35973.

27   B. M. Liszka, A. T. M. Lenferink, G. J. Witkamp and C. Otto, *J. Raman Spectrosc.*, 2015, **46**, 1230–1234.

28   G. El-Hajje, C. Momblona, L. Gil-Escrig, J. Ávila, T. Guillemot, J.-F. Guillemoles, M. Sessolo, H. J. Bolink and L. Lombez, *Energy Environ. Sci.*, 2016, **9**, 2286–2294.

29   T. Abraha, J. Cheng, W.-N. Su, C.-J. Pan, M. Tsai, H.-M. Chen, Z. Yang, H. Tan, C.-H. Chen, M.-H. Yeh, A. G. Tamirat, H.-F. Huang, L.-Y. Chen, J.-F. Lee, Y.-F. Liao, E. H. Sargent, H. Dai and B. J. Hwang, *J. Mater. Chem. A*, 2017, **5**, 21002–21015.

30   Y. Shao, Z. Xiao, C. Bi, Y. Yuan and J. Huang, *Nat. Commun.*, 2014, **5**, 1–7.

31   M. L. Petrus, Y. Hu, D. Moia, P. Calado, A. M. A. Leguy, P. R. F. Barnes and P. Docampo, *ChemSusChem*, 2016, **9**, 2699–2707.

32   Z. Song, A. Abate, S. C. Watthage, G. K. Liyanage, A. B. Phillips, U. Steiner, M. Graetzel and M. J. Heben, *Adv. Energy Mater.*, 2016, **6**, 1–7.
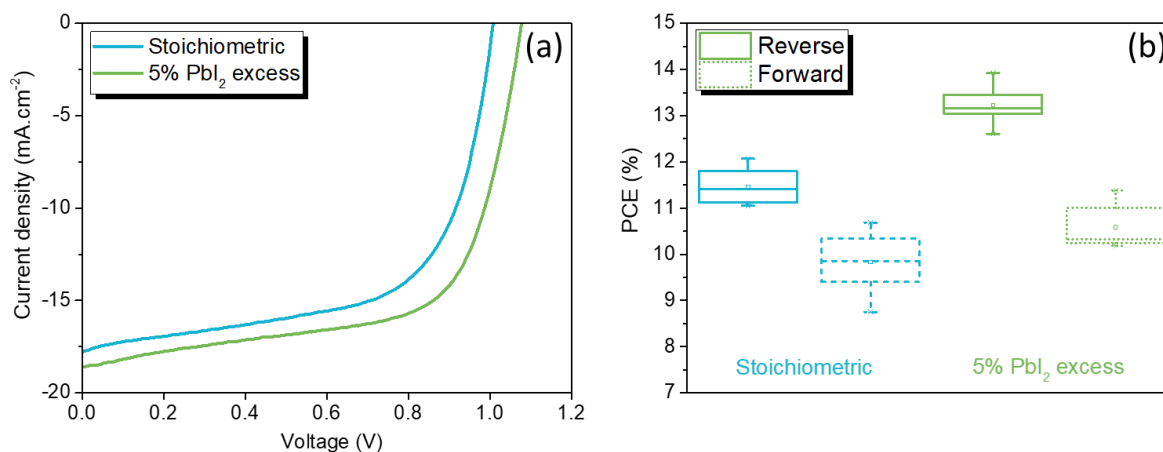
Supplementary information

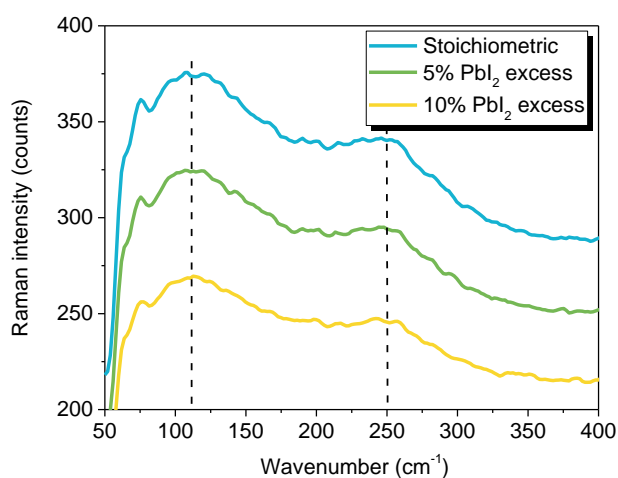**Fig. S1.** Experimental set-up used for Raman-photocurrent-photoluminescence mapping

Fig. S2. (a) PbI₂ film thickness as a function of concentration. **(b)** Raman spectra of PbI₂ thin films on glass with different thicknesses. **(c)** PbI₂ Raman intensity integrated between 80 cm^{-1} and 140 cm^{-1} as a function of film thickness. The dotted line is a polynomial fit of experimental data.
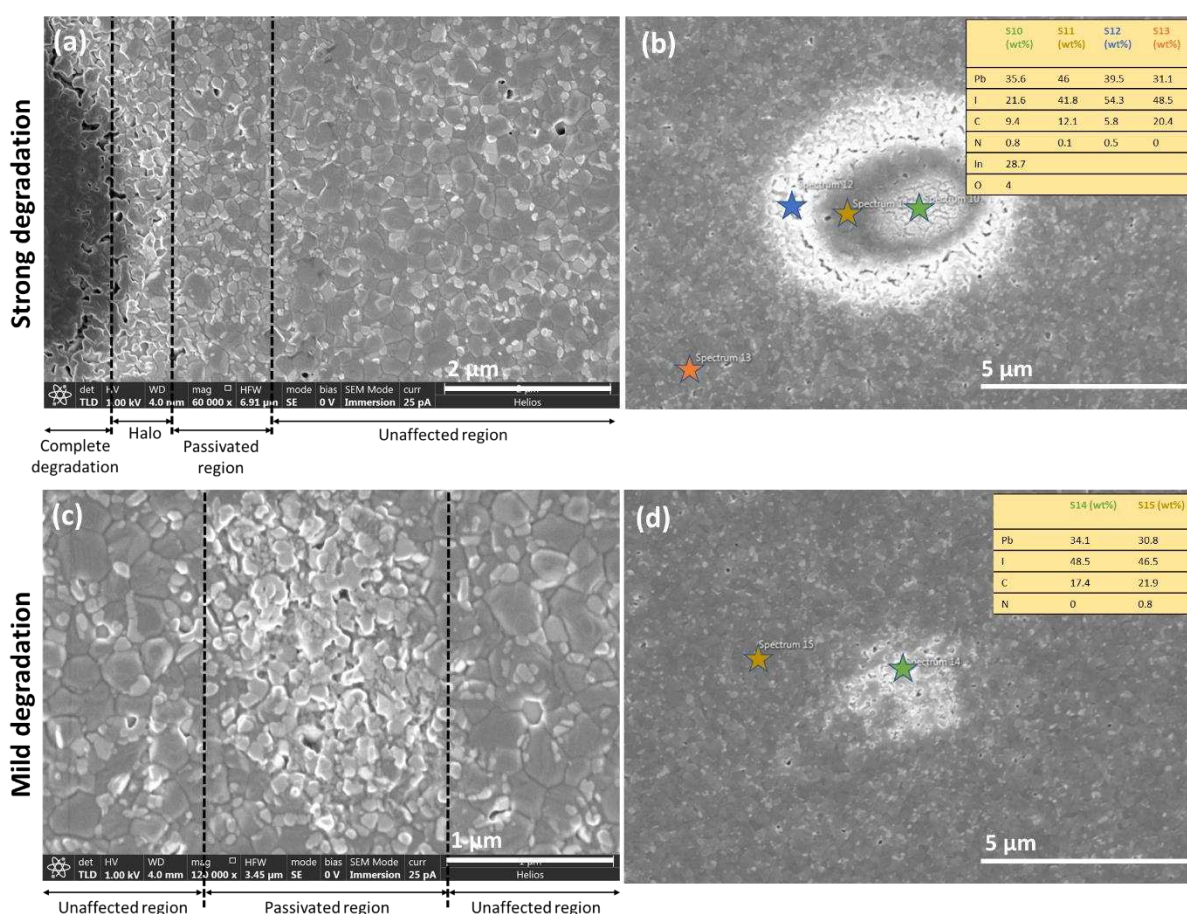
Fig. S3. (a) Typical J-V curves of perovskite solar cells with structure glass/ITO/NiOₓ/CH₃NH₃PbI₃/PCBM/BCP/Ag using stoichiometric or 5% PbI₂ excess perovskite solution. (b) statistical power conversion efficiency data for 10 different devices having stoichiometric or 5% PbI₂ excess perovskite.

Fig. S4. Raman spectra of MAPbI₃ films on ITO/glass substrates prepared with different amounts of PbI₂ excess. Each spectrum is an average of 200 data points measured using laser power of 0.15 mW for 10 s.

Fig. S5. high and low magnification SEM top-view images of perovskite films degraded with (a-b) 0.03 mW laser power for 120 s and (c-d) 0.3 mW laser power for 120 s in air, with corresponding Energy Dispersive Spectroscopy (EDS) measurements taken at various locations along the degraded spot (b and d).